New nanostructured electrochemical biosensors based on three-dimensional (3-mercaptopropyl)-trimethoxysilane network

A. M. Parra-Alfambra,[a] E. Casero,*[a] M. D. Petit-Domínguez,[a] M. Barbadillo,[a] F. Pariente,[a] L. Vázquez[b] and E. Lorenzo*[a]

Received 5th July 2010, Accepted 30th September 2010
DOI: 10.1039/c0an00475h

The design and characterization of a new nanostructured organic–inorganic hybrid material and its application to L-lactic acid determination are described. This material is based on the integration of the enzyme lactate oxidase (LOx) and gold nanoparticles (AuNPs) into a sol–gel 3D polymeric network derived from (3-mercaptopropyl)-trimethoxysilane (MPTS) previously formed onto a gold surface. MPTS presents the advantage of forming a 3D polymeric network containing a large number of thiol tail groups distributed throughout its structure that enable both its anchoring onto gold surfaces and the AuNPs incorporation. Moreover, this matrix provides a biocompatible environment that preserves the catalytic activity of LOx after its immobilization and allows the incorporation of a high amount of enzyme, which is expected to improve the sensitivity of the final biosensing device. Characterization of the designed biosensing platform was performed using quartz crystal microbalance (QCM), scanning electron microscopy (SEM) and atomic force microscopy (AFM) techniques. From the conjunction of these techniques, information about (i) the kinetic of LOx adsorption process in real time, (ii) the amount of LOx incorporated into the network, and (iii) the morphological characteristics at the nanometre level of the designed biosensing material was obtained. This information is very useful on the development of successful biosensing devices. Finally, the response of the biosensor to L-lactic acid was evaluated. The biosensor responds linearly to L-lactic acid in the range of 50 μM to 0.25 mM, with a sensitivity of 3.4 μA mM^{-1} and a detection limit of 4.0 μM.

Introduction

The use of different strategies for developing three-dimensional polymeric networks to produce new materials has been of great interest in the design of new bioanalytical devices such as biosensors in the last years. In particular, the employment of a polymeric network generated by sol–gel technology has been widely used as an adequate matrix in which several compounds, including biological material, can be encapsulated giving rise to a biosensor device.[1–3] This matrix provides not only a substrate which allows the encapsulation of high amount of enzyme but also a biocompatible environment that preserves the catalytic activity of the enzyme after the immobilization step, which are important issues in the field of biosensors development.[4,5] Moreover, the sol–gel network is simple to prepare and presents important properties, mainly its chemical inertness, high stability, physical rigidity, a renewable surface and tuneable properties.[6,7] Among the different precursors that have been reported in the literature for the sol–gel network preparation, the most employed for enzyme encapsulation are oxysilanes such as methyltrimethoxysilane, tetramethoxysilane, 3-aminopropyltriethoxysilane and tetraethoxysilane.[8–16] In this sense, an interesting precursor that can be used in the sol–gel network generation is the (3-mercaptopropyl)-trimethoxysilane (MPTS). MPTS is known to form a 3D structure, plenty of thiol tail groups with a strong affinity to gold,[17] by hydrolysis and condensation processes.[18,19] Thanks to the thiols groups, distributed throughout the network, MPTS is able not only to chemisorb onto gold surfaces but also to conveniently link nanosized Au particles.[20–22]

Recently, the employment of nanomaterials in the development of biosensor platforms has attracted increasing research attention as a strategy to improve the analytical properties of these devices.[3,20,21,23–28] Particularly, gold nanoparticles (AuNPs) have been used in a wide range of applications due to their chemical stability and interesting physicochemical properties,[20,21] such as a large surface area and an excellent biocompatibility. In particular, recent advances have been made to improve the charge transport in bio-sol–gels, which has been achieved through the addition of metal nanoparticles or carbon nanotubes.[18,29]

The development of methods for the determination of L-lactic acid is of great importance in several areas such as medicine and food industry.[30–36] From a medical point of view, the determination of L-lactic acid concentration in blood is essential because it is related to several diseases such as shocks, respiratory insufficiency and heart failure. Moreover, it allows also the diagnosis of patient conditions during intensive care and surgical operation process, as well as the estimation of the conditions of athletes. In food industry, the L-lactic acid level is an indicator of the fermentative process and it is related to freshness, stability and storage quality of several products. Our efforts over the past years in this field have been addressed to design L-lactic acid biosensors based on

[a]*Departamento de Química Analítica y Análisis Instrumental, Facultad de Ciencias, C/Francisco Tomás y Valiente N°7, Campus de Excelencia de la Universidad Autónoma de Madrid, 28049 Madrid, Spain. E-mail: encarnacion.lorenzo@uam.es; elena.casero@uam.es*
[b]*Instituto de Ciencia de Materiales de Madrid (CSIC), C/Sor Juana Inés de la Cruz N°3, Campus de Excelencia de la Universidad Autónoma de Madrid, 28049 Madrid, Spain*

lactate oxidase (LOx) enzyme immobilization onto gold substrates. Among the different available strategies to achieve the enzyme immobilization we have focused our attention on (i) LOx adsorbed directly onto a gold surface (Au/LOx) and (ii) LOx immobilized onto gold surfaces previously modified with a bifunctional reagent containing succinimide functionalities, in particular, 3,3′-dithiodipropionic acid di(*N*-succinimidyl ester) (DTSP).[35] The interactions responsible for enzyme immobilization are unspecific adsorption and covalent bonding, respectively. The response of both biosensors was obtained by replacing the natural electron acceptor (O_2) by an artificial mediator (hydroxymethylferrocene, HMF), whose electrochemical behaviour is followed at +0.30 V, instead of detecting the hydrogen peroxide generated in the following reaction:

$$\text{Lactate} + O_2 \rightarrow \text{Pyruvate} + H_2O_2$$

This strategy allows minimizing the contribution of interfering substances that could be oxidized at the high potential required for H_2O_2 detection.

In the present work, we have developed a strategy to prepare a new nanostructured lactic acid electrochemical biosensor, denoted as Au/MPTS/AuNPs/LOx. It is based on the immobilization of LOx into a three-dimensional polymeric network generated from MPTS onto a gold surface, which also provides multi-attaching sites for the incorporation of AuNPs. This new organic–inorganic hybrid material (Au/MPTS/AuNPs/LOx) was designed with the aim of benefiting from their different components: (i) a three-dimensional polymeric network that provides a biocompatible environment for enzyme protection, (ii) gold nanoparticles contributing to facilitate normal electron transfer kinetics by acting as tiny conduction centers, and (iii) a recognition element, the enzyme, offering a high selectivity. Moreover, the employment of MPTS presents the advantage of forming a 3D polymeric network that is full of thiol tail groups distributed throughout the structure that serve for both anchoring it onto gold surfaces through a S–H bond and incorporating AuNPs. We have also paid close attention to characterize the different biosensor construction steps as well as the resulting device. Characterization of the designed biosensing platform was performed using quartz crystal microbalance (QCM), scanning electron microscopy (SEM) and atomic force microscopy (AFM) techniques. QCM was employed to follow the LOx adsorption process in real time, providing simultaneously kinetic information about the process as well as the amount of immobilized enzyme. SEM and AFM measurements were employed for the visualization of the surface platform, providing with morphological information at the nanometre level. Finally, the developed biosensor device was tested by measuring the electrochemical response towards L-lactic acid in the presence of a redox mediator, HMF, in solution and its performance was evaluated in terms of sensitivity, detection limit and linear response range.

Experimental

Reagents and materials

Lactate oxidase (EC 232-841-6 from Pediococcus species) was obtained from Sigma Chemical Co. (St Louis, MO). Stock solution was prepared by dissolving the LOx lyophilized powder in 400 μL of 0.1 M phosphate buffer (pH 7.0), aliquoted and stored at −30 °C. L-(+)-Lactic acid lithium salt (97%) and colloidal gold (20 nm particle size) were also purchased from Sigma Chemical Co. (3-Mercaptopropyl)-trimethoxysilane and hydroxymethylferrocene were provided from Aldrich. Other chemicals used in this work, such as sodium phosphate, tartaric acid, citric acid, glucose, fructose and ascorbic acid, were reagent grade quality and used as received without additional purification steps. Sodium phosphate was employed for the preparation of buffer solutions (0.1 M, pH = 7.0). Water was purified with a Millipore Milli-Q-System. All solutions were prepared just prior to use.

Experimental techniques

Scanning electron microscopy (SEM) measurements. The Scanning Electron Microscopy measurements were performed with a NOVA NANOSEM 230 equipment (FEI) operating with a VCD (low voltage–high contrast) detector that allows us to simultaneously detect the secondary and backscattered electron signals.

Atomic force microscopy (AFM) measurements. The atomic force microscope was a Nanoscope IIIa from Digital Instruments (DI, Santa Barbara, CA) used with D scanner (maximal scan range of ~14 μm). Measurements were carried out by using Si and silicon nitride cantilevers from Veeco. The samples were imaged with different cantilevers in order to ensure that the imaged structures were not due to tip artefacts. The samples were imaged in the dynamic mode under liquid environment.

Quartz crystal microbalance (QCM) measurements. AT-cut quartz crystals (5.0 MHz) of 25 mm diameter with Au electrodes deposited over a Ti adhesion layer (Maxtek Inc. Santa Fe Springs, CA) were used for QCM measurements. An asymmetric keyhole electrode arrangement was used, in which the circular electrode geometrical areas were 1.370 cm^2 (front side) and 0.317 cm^2 (backside). Prior to use, the quartz crystals were cleaned by immersion in piranha solution, H_2SO_4/H_2O_2 (3 : 1 v/v). They were subsequently rinsed with water and dried in air. The quartz crystal resonator was set in a probe (TPS-550, Maxtek) made of Teflon in which the oscillator circuit was included, and the quartz crystal was held vertically. The probe was connected to a cell by a homemade Teflon joint which was immersed in water-jacketed beaker thermostatted at the assay temperature (20.0 ± 0.1 °C) with a thermostatic bath (Digital Temperature Controller Haake F6). The frequency was measured with a plating monitor (PM-740, Maxtek Inc.) and simultaneously recorded by a personal computer. The admittance of the quartz crystal resonator was measured near its resonant frequency by an impedance analyzer (HP4194A, Hewlett-Packard) equipped with a test lead (HP16048A). A probe similar to that used in the QCM measurements, but which did not include an oscillator circuit inside, was used to accomplish a direct connection of the quartz crystal resonator to the impedance analyzer.

Electrochemical measurements. All electrochemical measurements were performed on an Ecochemie Autolab PGSTAT12 system (Utrecht, The Netherlands). Experiments were carried out in a three-compartment electrochemical cell with standard taper joints so that all compartments could be hermetically sealed with Teflon adapters. All potentials are reported against a Ag/AgCl (Metrohm, 3.0 M KCl) reference electrode. The auxiliary electrode was a platinum wire and modified-Au electrodes were used as the working electrode. Cyclic voltammetry (CV) and chronoamperometry were the electrochemical techniques applied to study the response of the designed biosensor in the presence of HMF (which acts as soluble mediator in solution) and in the presence or absence of L-lactic acid. Solutions were deaerated with nitrogen gas before use, and the gas flow was kept over the solutions during experiments.

Procedures

Electrode conditioning. Prior to modify the gold electrode, the surface was cleaned and activated as follows: gold electrodes were polished with 1 μm diamond paste (Buehler) and rinsed with water. Then, the electrodes were activated by holding the potential at +2.0 V for 5 s in 0.1 M H_2SO_4 and at −0.35 V for 10 s, followed by potential cycling from −0.20 V to +1.5 V at 5 V s^{-1} for 2 min. After this treatment, the cyclic voltammogram characteristic of a clean polycrystalline gold electrode was recorded (from −0.20 to +1.5 V) at 100 mV s^{-1}.

SEM and AFM supports conditioning. Gold supports employed for AFM and SEM measurements consisted of glass substrates (1.1 cm × 1.1 cm) covered with a chromium adhesion layer (1–4 nm thickness) in which a gold layer (200–300 nm thickness) was deposited (Arrandee Co. Werther, Germany). In both cases gold surfaces were previously annealed for 2 min in a gas flame in order to obtain Au (111) terraces. After the annealing procedure, the surface morphology of the gold substrates imaged by AFM displayed a granular morphology with lateral sizes of a few microns separated by relatively deep grooves. This morphology leads to a root mean square roughness, σ, in the 12–18 nm range. However, the surface of these grains is quite smooth and flat with σ in the 0.1–0.4 nm range. Moreover, the grain surface displayed the triangular facet arrangement typical of the Au (111) surfaces.[37]

QCM experiments. For monitoring the mass changes associated with the LOx incorporation into the sol–gel matrix, a QCM probe (a MPTS/AuNPs functionalized gold substrate) was immersed in 10 mL of phosphate buffer solution (pH = 7.0) and the frequency of the quartz crystal was monitored as a function of time. After the temperature and frequency had stabilized, an aliquot of the enzyme stock solution was added to the cell in order to obtain a final concentration of protein of 0.2 μM.

Sol–gel solution preparation. The sol–gel solution was prepared by mixing 200 μL of MPTS with 600 μL of water, 600 μL of methanol and 200 μL of 0.1 M HCl. This solution was sonicated using an Ultrasons bath (P-Selecta) for 30 min at room temperature and subsequently the solution was stored for three hours at room temperature.

Nanostructured biosensor preparation. The preparation of the biosensor, denoted as Au/MPTS/AuNPs/LOx, was carried out by immersing the activated electrode or the Arrandee Au support in the MPTS sol–gel solution, prepared as described above, for an hour. MPTS sol chemisorbs on the polycrystalline Au electrode forming a 3D silicate network.[20] The resulting MPTS sol-modified electrode was thoroughly rinsed with water to remove the physically adsorbed MPTS sol and immersed into colloidal AuNPs solution overnight at 4 °C. The nanosized Au particles chemisorb onto the thiol groups of the silicate network. The resulting MPTS/AuNPs-modified electrode was rinsed again with water and finally 10 μL of the LOx stock solution were dropped on this surface for three hours at 4 °C. The different steps involved in the biosensor preparation are summarized in Scheme 1.

Results and discussion

Biosensor development: optimization of parameters

The different steps involved in the preparation of the biosensing organic–inorganic hybrid material, see Scheme 1, were optimized. In order to achieve this goal, different conditions for preparing the biosensing material (sol–gel reagents amounts, time of the different processes) were assayed. As mentioned in the Experimental section, the first step of the biosensor fabrication consists of generating the polymeric network by sol–gel technology, in which all the components integrating the biosensor will be subsequently encapsulated. Since the final properties of the resulting three-dimensional matrix depend strongly on the composition of the sol–gel solution, several volume ratios of MPTS : H_2O : CH_3OH : HCl were tested. From this study, it was concluded that the optimal volume ratio to obtain a homogeneous and transparent solution after ultrasonic agitation was 1 : 3 : 3 : 1. Moreover, these conditions allow us to obtain sol–gel solutions without phase separation, relative short gelation times and adequate viscosity. The resulting sol–gel solution is settled for a given time before immersing the activated electrode in it. During this time, the hydrolysis and polycondensation reactions, responsible for the polymeric network generation, started. Several settle times, from 1 to 6 hours, were assayed in order to ascertain their influence in the biosensor response. An optimal time of 3 hours was selected because for this time the response of the biosensor towards L-lactic acid was maximum. Likewise, the optimal time for the electrode immersion in the as-prepared sol–gel solution was selected. In this case, the maximum biosensor response corresponded to an immersion time of 1 hour.

Biosensor characterization

In order to obtain reproducible responses it is essential to control the different steps followed for the construction of the biosensing platforms. In particular, the incorporation of both AuNPs and LOx onto the polymeric network must be carried out according to a systematic methodology. In this sense, the employment of SEM and AFM techniques, which allowed us to visualize the immobilized AuNPs and LOx, implies an important advance in order to achieve the control of the process. Therefore, once we selected the optimal conditions to prepare the biosensing platform, we performed SEM and AFM measurements of the

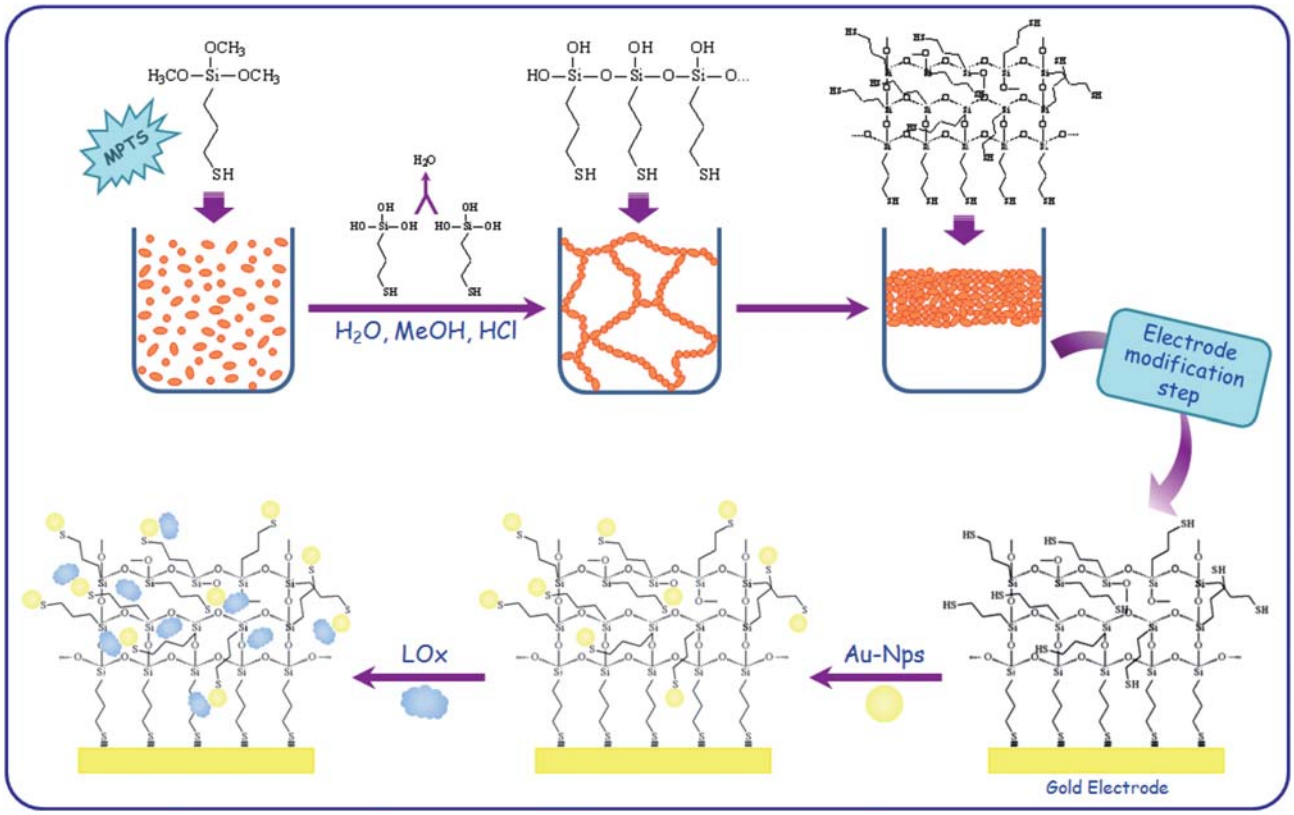

Scheme 1 Schematic representation of the different steps involved in the preparation of the biosensing organic–inorganic hybrid material and the corresponding electrode modification.

MPTS/AuNPs and MPTS/AuNPs/LOx modified gold surface, respectively. These experiments provide morphological information, allowing the characterization of the system at the nanoscale level. The SEM images, corresponding to the Au/MPTS (Fig. 1A) and the Au/MPTS/AuNPs (Fig. 1B) systems, show that gold nanoparticles have been successfully incorporated into the polymeric network. In Fig. 1A, the typical microgranular surface morphology of the annealed gold sample can be observed where large grains (with lateral sizes in the range of 1–5 microns) are clearly formed as a consequence of the annealing process. In Fig. 1B, the gold nanoparticles can be found scattered in the imaged area. The nanoparticles are not homogeneously distributed, since regions with a low particle concentration are detected together with other regions in which they almost form a continuous layer. A higher resolution SEM image (Fig. 1C) allows us to confirm the rather homogeneous size distribution of the Au nanoparticles since they present similar dimensions (21 $\pm$ 1.5 nm). However, SEM analysis does not allow us to detect the MPTS layer initially formed on top of the gold annealed surface.

Gold and Au/MPTS/AuNPs/LOx surfaces were imaged by AFM. Micron scale AFM image of the annealed gold surface (Fig. 1D) shows a morphological structure formed by large grains, with relatively deep grooves between them. Fig. 1E shows an AFM three dimensional view of the imaged topography taken on top of one of gold grains, but this time of the MPTS/AuNPs/LOx system. On top of the rather flat and granular (with lateral sizes in the 8–10 nm range) surface there are clear protrusions that correspond to the AuNPs. However, in this case the AuNPs are not featureless since they display a corrugated surface in which tiny structures can be distinguished. These structures together with those nanogranular ones observed on the surrounding flat surface correspond clearly to LOx structures, since they were only found on those samples where LOx was adsorbed. The above results clearly show that nanoparticles have been successfully incorporated into the polymeric network with a random distribution in the whole material. In addition, LOx has also immobilized not only on the AuNPs surface but also onto the MPTS surrounding flat surface.

In order to further characterize the resulting organic–inorganic designed material, we also carried out QCM measurements. This technique allows us to determine the amount of enzyme incorporated into the three dimensional polymeric network, as well as to obtain kinetic information about the LOx adsorption process.[38] As described in the Experimental section, this study was carried out in a cell coupled to the QCM probe containing the MPTS/AuNPs modified-Au quartz resonator in contact with 10 mL of buffer solution. After the temperature and the frequency were stabilized, an aliquot of LOx stock solution was added to the cell. As can be seen in Fig. 2, upon addition of LOx, the frequency decreased during 10 minutes until a steady state was reached. The measured ΔF value is 35 $\pm$ 0.3 Hz. The quantitative relationship between the relative shift of the resonant frequency and the added mass was derived by Sauerbrey equation[39] who assumed that, for small mass changes (less than

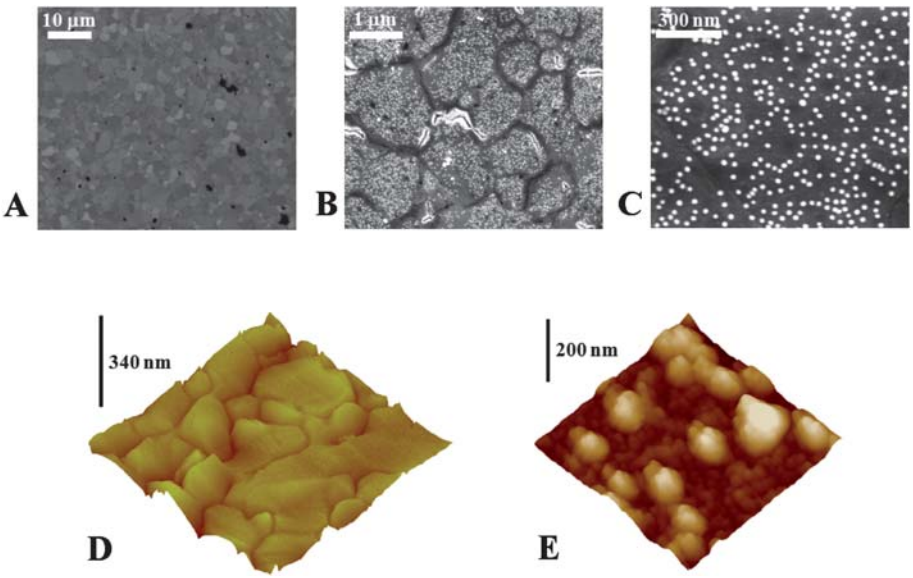

Fig. 1 SEM image taken on a relatively large area comprising several gold micrograins of a (A) Au/MPTS system and (B) Au/MPTS/AuNPS system. Note the inhomogeneous distribution of the gold nanoparticles. (C) Higher resolution SEM image taken on top of one of the gold micrograins where the individual AuNPs are clearly distinguished. Tapping mode AFM images obtained under liquid environment of (D) an annealed gold substrate (5.34 × 5.34 μm^2) and (E) a Au/MPTS/AuNPs/LOx sample surface (338 × 338 nm^2).

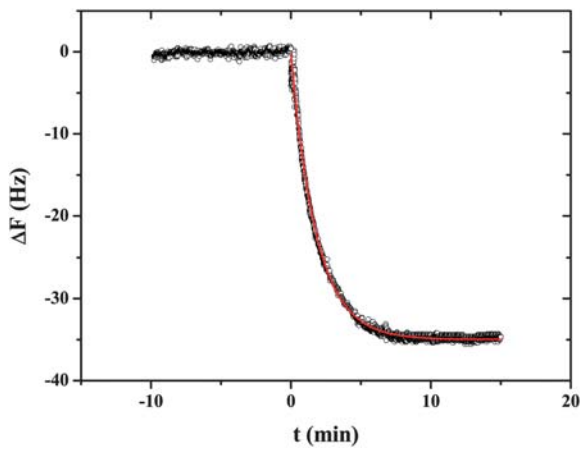

Fig. 2 Time dependence of the frequency changes of a MPTS/AuNPs modified gold surface resonator in 0.1 M phosphate buffer solution upon addition of lactate oxidase to a final concentration of 0.2 μM.

2% of the crystal mass), the added mass is treated as an added thickness of the crystal itself.

$$\Delta f = -2f^2\Delta m/A(\mu\rho_q)^{0.5} \quad (1)$$

where Δf is the measured resonant frequency shift (Hz), f is the intrinsic crystal frequency, Δm is the added mass (g), A is the area (cm^2) of the quartz plate (between the two electrodes of opposite faces), ρ_q is the density of quartz (2.65 g cm^{-3}), and μ is the shear modulus (2.95 × 10^{11} dyn cm^{-2}). The negative sign in eqn (1) indicates that an addition of mass to the resonator results in a decrease in its resonant frequency and *vice versa*.

Eqn (1) can be simplified as follows:

$$\Delta m = -C_f\Delta F \quad (2)$$

where C_f is a proportionality constant, whose value for the 5.0 MHz crystals used in this study is 17.7 ng Hz^{-1} cm^{-2}. However, it is important to note that whether the measurement is performed in liquid environments both mass and liquid loading contribute to the total frequency changes. In addition, since the frequency change is affected by both density and viscosity of the liquid, QCM also responds to viscosity changes produced when samples are injected. In particular, biomolecules usually lead to considerable alterations of the viscoelastic properties near the sensor surface, which renders inadequate the employment of the Sauerbrey equation.[40] In this sense, in order to confirm that in the present case, there are not considerable alterations of the viscoelastic properties near the resonator, an impedance analysis was carried out. Admittance measurements of the quartz crystals were obtained during the immobilization of the LOx, following the same procedure as the one used to measure the frequency decrease. During the experiment the resistance parameter of the equivalent electric circuit remains constant as a function of time (data not shown). This demonstrates that the main factor giving rise to the frequency changes is a change in the mass of the resonator, so, therefore, frequency and mass changes can be correlated and eqn (1) is applicable. According to eqn (2), the amount of LOx incorporated to the network was 619 ± 4 ng cm^{-2}. Moreover, from the shape of the frequency-time profile the kinetics of adsorption can be studied. The overall process can be controlled by either transport (diffusion) or by kinetics (activation controlled), which predict time dependencies of $t^{1/2}$ and exp(t), respectively. Assuming that the immobilization process is kinetically controlled, experimental data were fit (Fig. 2, solid line) to a first-order kinetics equation:

$$\Delta F = \Delta F_{max}(1 - e^{-kt}) \quad (3)$$

where ΔF is the frequency change (in Hz), ΔF_{max} is the frequency change between the initial and the final steady-state frequencies,

Table 1 First order rate constant (k), frequency change (ΔF_{max}), and mass (m) for the immobilization process of LOx onto (A) a MPTS/AuNPs modified gold resonator, (B) a bare gold resonator and (C) a DTSP modified gold resonator

	k/min^{-1}	ΔF_{max}/Hz	m/ng cm^{-2}
(A) Au/MPTS/AuNPs/LOx	0.55	−35.0	619
(B) Au/LOx	0.22	−9.9	176
(C) Au/DTSP/LOx	0.04	−10.2	180

and k is the first-order rate constant expressed in min^{-1}. The values obtained from the experimental data fit for ΔF_{max} and k are −35 Hz and 0.55 min^{-1}, respectively. These values together with the mass change (m), obtained from the Sauerbrey equation, are summarized in Table 1. In order to study the influence of the polymeric network in both the loading and the kinetics adsorption of the enzyme, the ΔF_{max}, k and m values obtained when LOx has been immobilized (i) onto a bare gold surface (Au/LOx) and (ii) onto a gold surface previously modified with the bifunctional reagent 3,3′-dithiodipropionic acid di(*N*-succinimidyl ester) (DTSP)[35] were also displayed in Table 1. From the comparison of the ΔF_{max} values obtained for the three different immobilization strategies, it can be concluded that the existence of a polymeric network allows the encapsulation of a LOx amount 3.5 times higher than that obtained by the two other strategies. Moreover, from the different values obtained for the constant (k), it is evident that the frequency decreases at a different rate depending on the system under study. The difference in the kinetics of adsorption may be explained as a consequence of the different mechanisms involved in the enzyme immobilization for Au/LOx, Au/DTSP/LOx and Au/MPTS/AuNPs/LOx systems, respectively. On a bare gold resonator, the adsorption of LOx occurs with a random distribution of protein adsorption geometries. Oppositely, when the immobilization of LOx takes place onto a DTSP modified gold resonator, a particular orientation of the enzyme is required. In this case, formation of a covalent binding implies that the LOx amine groups must be oriented to the surface, in which the terminal *N*-succinimidyl esters of the DTSP monolayer are exposed to the solution. Finally, the faster kinetics corresponds to the Au/MPTS/AuNPs/LOx system since the 3D configuration offers higher binding sites to entrap the enzyme.

Biosensor response

The biosensor response is based on the oxidation of lactate to pyruvate, catalyzed by LOx, in the presence of HMF which acts as soluble mediator in solution. Fig. 3A displays the cyclic

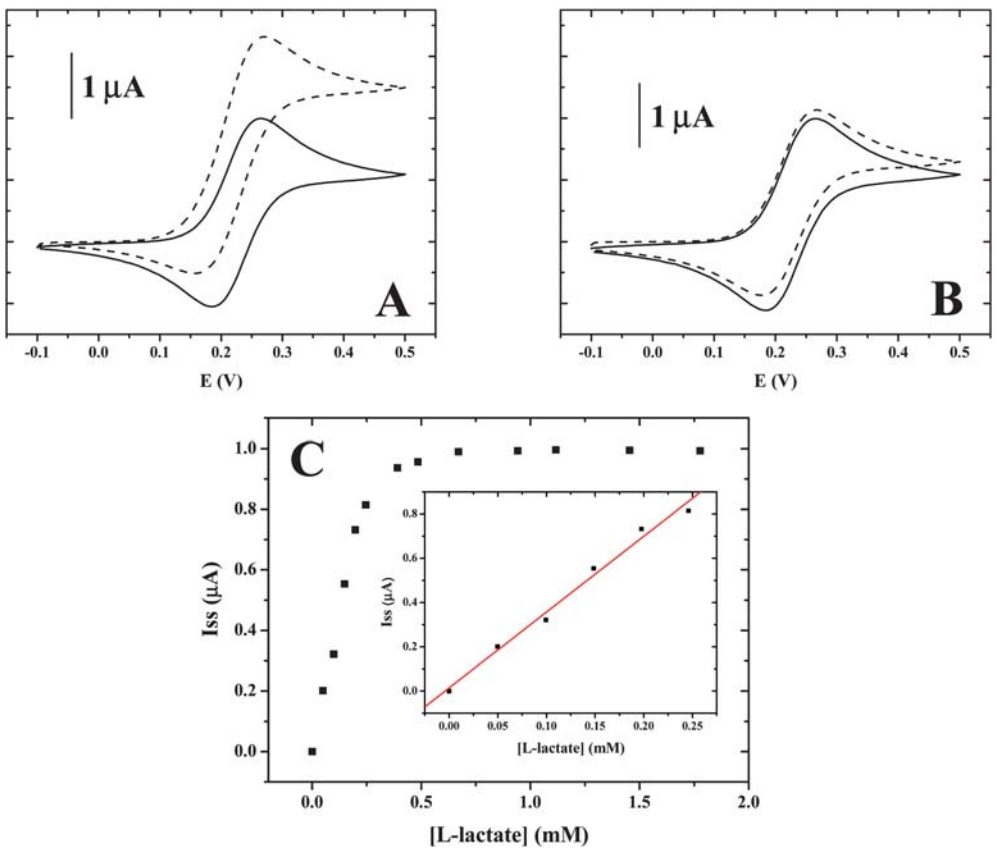

Fig. 3 Cyclic voltammetric response for (A) Au/MPTS/AuNPs/LOx and (B) Au/MPTS/LOx platforms in contact with a 0.1 M phosphate buffer solution containing 1.0 mM hydroxymethylferrocene in the absence (solid curves) and in the presence (dashed curves) of 1.0 mM of lactate. The scan rate was 10 mV s^{-1}. (C) Calibration curve obtained from chronoamperometric measurements (E = +0.30 V) for Au/MPTS/AuNPs/LOx platform in contact with a 0.1 M phosphate buffer solution containing 1.0 mM hydroxymethylferrocene in the presence of increasing amounts of lactate. The inset shows the linear range.

voltammetric response from −0.1 to +0.5 V at 10 mV s^{-1} for Au/MPTS/AuNPs/LOx biosensor in contact with a 0.1 M, pH 7.0, phosphate buffer solution containing 1.0 mM hydroxymethylferrocene in the absence (solid curve) and in the presence (dashed curve) of lactic acid. As can be seen, in the absence of lactic acid, the typical redox response of the ferrocene/ferrocinium process in aqueous media is observed. Upon addition of lactic acid to a final concentration of 1 mM, there is an enhancement of the anodic peak current concomitant with a decrease of the cathodic peak current, which is consistent with a clear electrocatalytic effect. To confirm the role of the enzyme in the catalytic response, the cyclic voltammetric response of a Au/MPTS/AuNPs electrode was obtained in the same conditions (data not shown). As one would expect upon addition of lactic acid no catalytic waves were observed.

As mentioned above, we have employed gold nanoparticles with the aim of improving charge transport in the designed organic–inorganic hybrid material. In order to assess if we have achieved this goal, we have determined the influence of the AuNPs on the response by obtaining the cyclic voltammograms of a Au/MPTS/LOx biosensor (Fig. 3B) in the absence (solid curve) and in the presence (dashed curve) of 1 mM lactic acid. From comparison of the catalytic current obtained for both systems, with and without AuNPs, it is evident that, as one would expect, the employment of AuNPs in the biosensor construction enhances significantly the analytical response of the resulting device.

In order to obtain the analytical properties of the Au/MPTS/AuNPs/LOx biosensor, chronoamperometric experiments were carried out at a potential of +0.30 V, where oxidation of HMF by the electrode is assured. Fig. 3C displays typical calibration curves obtained from these measurements. The analytical properties—linear response, sensitivity, detection limit, reproducibility, and repeatability—are summarized in Table 2. As shown in Fig. 3C, the calibration plot was linear from 50 μM to 0.25 mM concentration range ($r = 0.994$). The sensitivity value, calculated from the slope of the plot, was of 3.4 μA mM^{-1}. The detection limit, calculated as the ratio between three times the standard deviation of background current and the sensitivity, was 4.0 μM. The repeatability was evaluated from the relative standard deviation (RSD) of ten different measurements of a 0.1 mM lactate concentration with the same biosensor. An RSD value of 2% was obtained. The reproducibility using three different biosensors was 5%. As can be seen in Table 2, most of the analytical properties corresponding to Au/MPTS/AuNPs/LOx biosensor are comparable or even better than those reported in the literature for similar sol–gel-based lactate biosensors.

One of the main goals on developing three-dimensional polymeric network based bioanalytical platforms is to provide a biocompatible environment that preserves the catalytic activity of the biomolecule after the immobilization step. In order to assess if it is the case of the developed three dimensional polymeric network, the storage stability of the resulting lactate biosensor was investigated by measuring the magnitude of the current response for a 0.1 mM lactate concentration every day, keeping the biosensor stored at 4 °C between measurements. When the biosensor is reused, a decay in the signal of 10% of the initial response is observed after 10 days.

Finally, we have carried out a study of the influence of the more usual potential interferents. In this sense, we have obtained the biosensor response in the presence of several substances, which can act as interferences such as tartaric acid, citric acid, ascorbic acid, glucose and fructose. In order to test the effect of the mentioned substances, we have compared the biosensor response towards 0.1 M of lactic acid in the absence and in the presence of 0.1 mM of the potential interferent. The presence of the interfering compounds studied did not change the biosensor response except in the case of ascorbic acid. However, at lower concentration (10 μM) the presence of this compound did not show any effect. Therefore, these results suggest that the proposed device can be successfully used to measure lactate concentrations in the presence of a variety of possible interfering substances.

Conclusions

In this paper, we have developed and characterized a new nanostructured organic–inorganic hybrid material based on the

Table 2 Analytical properties of several biosensors reported in the literature for lactic acid detection including the present work. MPTS: (3-mercaptopropyl)-trimethoxysilane, AuNPs: gold nanoparticles, LOx: lactate oxidase, GC: glassy carbon, TEOS: tetraethoxysilane, PtNPs: Pt nanoparticles, CNTs: carbon nanotubes, MnO_2 NPs: MnO_2 nanoparticles, CoPh: cobalt phthalocyanine colloid, LDH: lactate dehydrogenase, and DTSP: 3,3′-dithiodipropionic acid di(*N*-succinimidyl ester)

Biosensor	Sensitivity/ μA mM^{-1}	Linear range/mM	Detection limit/μM	Repeatability (RSD) (%)	Reproducibility (RSD) (%)
Au/MPTS/AuNPs/LOx (present work)	3.4	0.05–0.25	4.0	2	5
GC/TEOS/PtNPs/CNTs/LOx (Huang *et al.*, 2008)	6.36	0.25–2.0	0.3	<2	—
GC/TEOS/CNTs/LOx (Huang *et al.*, 2007)	6.031	0.2–2.0	0.3	—	3.6
GC/chitosan/MnO_2NPs/CoPh/LOx (Wang *et al.*, 2006)	3.98	0.020–4.0	8	—	4.6
Au/PtNPs/mediator/LOx (Liu *et al.*, 2009)	1.43	1–20	—	—	5.5
Au/MPTS/AuNPs/LDH (Jena *et al.*, 2006)	0.447	0.1–0.6	20	—	—
Au/LOx (Parra *et al.*, 2006a)	0.77	Up to 0.3	10	1	8
Au/DTSP/LOx (Parra *et al.*, 2006a)	0.69	Up to 0.2	40	0.5	8

integration of LOx and AuNPs into a sol–gel 3D polymeric network derived from MPTS that is formed onto a gold surface. Thanks to the presence of thiol tail groups distributed throughout the MPTS structure, the network not only preserves the catalytic activity of the enzyme but also enables both its anchoring onto Au surfaces and the AuNPs incorporation. From AFM and SEM measurements, it was assessed that AuNPs are not homogeneously distributed over the area under study and that LOx molecules were found on both the AuNPs and the smoother MPTS surrounding areas. From QCM measurements it was concluded that the existence of a polymeric network allows the encapsulation of a higher LOx amount than that formerly obtained for other lactate biosensor where LOx has been immobilized following a different strategy. Moreover, differences in the kinetics of LOx adsorption were also observed. The electrocatalytic response of the Au/MPTS/AuNPs/LOx biosensor shows a linear dependence on the concentration of lactate in solution. The analytical properties of the biosensing platform were studied, obtaining a linear response in the range of 50 μM to 0.25 mM, a sensitivity value of 3.4 μA mM^{-1} and a detection limit of 4.0 μM. Finally, the Au/MPTS/AuNPs/LOx biosensor exhibits a better response when compared with the same biosensing platform but free of AuNPs (Au/MPTS/LOx).

Acknowledgements

This work has been supported by Comunidad Autónoma de Madrid (project No. S2009/PPQ-1642, AVANSENS), Comunidad Autónoma de Madrid/Universidad Autónoma de Madrid (project CCG08-UAM/SEM-4074) and Ministerio de Ciencia e Innovación (projects No. CTQ2008-05775, FIS2009-12964-C05-04 and Consolider No. CSD2007-00010).

References

1 L. Rabinovich and O. Lev, *Electroanalysis*, 2001, **13**, 265–275.
2 W. Jin and J. D. Brennan, *Anal. Chim. Acta*, 2002, **461**, 1–36.
3 M. Barbadillo, E. Casero, M. D. Petit-Domínguez, L. Vázquez, F. Pariente and E. Lorenzo, *Talanta*, 2009, **80**, 797–802.
4 S. Braun, S. Rappoport, R. Zusman, D. Avnir and M. Ottolenghi, *Mater. Lett.*, 1990, **10**, 1–5.
5 H. Frenkel-Mullerad and D. Avnir, *J. Am. Chem. Soc.*, 2005, **127**, 8077–8081.
6 G. Cabello-Carramolino and M. D. Petit-Domínguez, *Anal. Chim. Acta*, 2008, **614**, 103–111.
7 G. Cabello-Carramolino and M. D. Petit-Domínguez, *Microchim. Acta*, 2009, **164**, 405–410.
8 B. Lillis, C. Grogan, H. Berney and W. A. Lane, *Sens. Actuators, B*, 2000, **68**, 109–114.
9 C. I. Li, Y. H. Lin, C. L. Shih, J. P. Tsaur and L. K. Chau, *Biosens. Bioelectron.*, 2002, **17**, 323–330.
10 J. A. Cox, P. M. Hensley and C. L. Loch, *Microchim. Acta*, 2003, **142**, 1–5.
11 A. Salimi, R. G. Compton and R. Hallaj, *Anal. Biochem.*, 2004, **333**, 49–56.
12 A. Kumar, R. R. Pandey and B. Brantley, *Talanta*, 2006, **69**, 700–705.
13 R. Pauliukaite, A. M. C. Paquim, A. M. Oliveira-Brett and C. M. A. Brett, *Electrochim. Acta*, 2006, **52**, 1–8.
14 S. Singh, R. Singhal and B. D. Malhotra, *Anal. Chim. Acta*, 2007, **582**, 335–343.
15 H. D. Duong and J. I. Rhee, *Talanta*, 2007, **72**, 1275–1282.
16 E. I. Yashina, A. V. Borisova, E. E. Karyakina, O. I. Shchegolikhina, M. Y. Vagin, D. A. Sakharov, A. G. Tonevitsky and A. A. Karyakin, *Anal. Chem.*, 2010, **82**, 1601–1604.
17 H. O. Finklea, in *Electroanalytical Chemistry*, ed. A. J. Bard and I. Rubinstein, Marcel-Decker, New York, 1996, vol. 19, pp. 109–135.
18 J. B. Jia, B. Q. Wang, A. G. Wu, G. J. Cheng, Z. Li and S. J. Dong, *Anal. Chem.*, 2002, **74**, 2217–2223.
19 X. Cheng and G. S. Wilson, *Langmuir*, 2004, **20**, 8762–8767.
20 B. K. Jena and C. R. Raj, *Anal. Chem.*, 2006, **78**, 6332–6339.
21 B. K. Jena and C. R. Raj, *Electroanalysis*, 2007, **19**, 816–822.
22 S. P. Gomes, M. Odlozilikova, M. G. Almeida, A. N. Araujo, C. M. C. M. Couto and M. C. B. S. M. Montenegro, *J. Pharm. Biomed. Anal.*, 2007, **43**, 1376–1381.
23 K. Wang, J. J. Xu and H. Y. Chen, *Sens. Actuators, B*, 2006, **114**, 1052–1058.
24 J. Huang, Z. Song, J. Li, Y. Yang, H. Shi, B. Wu, J. Anzai, T. Osa and Q. Chen, *Mater. Sci. Eng., C*, 2007, **27**, 29–34.
25 J. Huang, J. Li, Y. Yang, X. Wang, B. Wu, J. Anzai, T. Osa and Q. Chen, *Mater. Sci. Eng., C*, 2008, **28**, 1070–1075.
26 J. J. Cheng, J. W. Di, J. H. Hong, K. A. Yao, Y. B. Sun, J. Y. Zhuang, Q. Xu, H. E. Zheng and S. P. Bi, *Talanta*, 2008, **76**, 1065–1069.
27 T. García, E. Casero, M. Revenga-Parra, J. Martín-Benito, F. Pariente, L. Vázquez and E. Lorenzo, *Biosens. Bioelectron.*, 2008, **24**, 184–190.
28 C. X. Liu, H. M. Liu, Q. D. Yang, Q. Tian and X. X. Cai, *Chin. J. Anal. Chem.*, 2009, **37**, 624–628.
29 H. Chen and S. Dong, *Biosens. Bioelectron.*, 2007, **22**, 1811–1815.
30 B. Serra, A. J. Reviejo, C. Parrado and J. M. Pingarrón, *Biosens. Bioelectron.*, 1999, **14**, 505–513.
31 N. G. Patel, A. Erlenkotter, K. Cammann and G. C. Chemnitius, *Sens. Actuators, B*, 2000, **67**, 134–141.
32 R. Garjonyte, Y. Yigzaw, R. Meskys, A. Malinauskas and L. Gorton, *Sens. Actuators, B*, 2001, **79**, 33–38.
33 B. D. Malhotra and A. Chaubey, *Sens. Actuators, B*, 2003, **91**, 117–127.
34 S. Suman, R. Singhal, A. L. Sharma, B. D. Malhotra and C. S. Pundir, *Sens. Actuators, B*, 2005, **107**, 768–772.
35 A. Parra, E. Casero, L. Vázquez, F. Pariente and E. Lorenzo, *Anal. Chim. Acta*, 2006, **555**, 308–315.
36 A. Parra, E. Casero, L. Vázquez, J. Jin, F. Pariente and E. Lorenzo, *Langmuir*, 2006, **22**, 5443–5450.
37 E. Casero, M. Darder, F. Pariente, E. Lorenzo, J. Martín-Benito and L. Vázquez, *Nano Lett.*, 2002, **2**, 577–582.
38 E. Casero, A. M. Parra-Alfambra, L. Vázquez and E. Lorenzo, *Analyst*, 2010, **135**, 1878–1903.
39 G. Sauerbrey, *Z. Phys.*, 1959, **155**, 206–222.
40 G. N. M. Ferreira, A. C. da-Silva and B. Tomé, *Trends Biotechnol.*, 2009, **27**, 689–697.